MECHANICAL PERFORMANCE OF CARBON-FIBRE AND GLASS-FIBRE-REINFORCED EPOXY I-BEAMS: II. FRACTOGRAPHIC FAILURE OBSERVATIONS

M. D. Gilchrist,[a] A. J. Kinloch[b] & F. L. Matthews[c]

[a]*Mechanical Engineering Department, University College Dublin, Belfield, Dublin 4, Republic of Ireland*
[b]*Mechanical Engineering Department, Imperial College, Exhibition Road, London SW7 2BX, UK*
[c]*Centre for Composite Materials, Imperial College, Prince Consort Road, London SW7 2BY, UK*

Abstract

This present paper is the second in a series which together detail the static behaviour, fractographic observations, fatigue behaviour and finite element predictions of composite I-beams subjected to mechanical loads. Fractographic observations associated with the mechanical behaviour under static load of both unnotched and web- and flange-notched continuously reinforced carbon-fibre/epoxy and E-glass-fibre/epoxy I-beams are discussed. Ultrasonic scanning, X-radiography and both optical and scanning electron microscopy have been used to elucidate the presence of different damage mechanisms and the directions of delamination growth in different regions of the beams. The principal damage mechanisms which have been identified as causing failure are delamination, matrix cracking, splitting and fibre fracture.

As discussed in detail in the previous paper, a four-point flexural configuration was used. A mode of buckling that was antisymmetric across the width of the compressive flange was observed prior to failure in all cases. Failure of the unnotched I-beams initiated from a buckle on the compressive flange and the subsequent damage was predominantly in the form of delamination. The main delaminations were along the interfaces between the separate sub-components which comprise the I-beams: namely, the flange caps and C-sections and the backs of the two C-sections. These are all −45°/+45° interfaces, i.e. the relative fibre angle between the adjacent plies is 90°. Failure of the notched I-beams initiated from a shear-loaded circular cutout within the web. The critical damage mechanism was matrix cracking in local 90°/90° plies which were subject to local tensile stresses. Fibre fracture and component failure resulted from this matrix cracking.

Keywords: I-beam, carbon- and glass-fibre composites, flexure, buckling, fracture, interlaminar stress, delamination, fractography

NOTATION

E	Young's modulus
G	Shear modulus
PEEK	Poly(ether ether ketone) (matrix material)
PES	Poly(ether sulphone) (matrix material)
SEM	Scanning electron microscope
X	Strength
ν	Poisson's ratio

Subscripts

L	Longitudinal (laminate property dependent upon stacking sequence)
Lten	Longitudinal tensile
T	transverse (laminate property dependent upon stacking sequence)
Tten	Transverse tensile
11	Longitudinal (unidirectional ply property)
22	Transverse (unidirectional ply property)

1 INTRODUCTION

If successfully used, fractographic techniques can identify damage initiation sites and subsequent directions of propagation within structural components. Various damage mechanisms can readily be established and modes of failure or the mixity of different modes may also be calculated. Purslow[1–4] explained how the basic nodular structure of epoxy resin grows in a certain direction and on a particular plane with a characteristic featherlike appearance. The interaction of adjacent fracture planes appears as 'river' markings. The confluence of the 'rivers' indicates the direction of crack propagation. These fracture surfaces abut adjacent fractures which themselves may lie in different planes: such boundaries are larger than rivers and are termed scarps. Cusps or hackles are associated with regions of shear

and they can define the loading direction, i.e. the direction in which opposite fracture faces move relative to each other.[5–7] Moreover, the amount of shear relative to tensile opening, i.e. mode II/I loading, can be related to the steepness of the shear cusp, which is particularly useful for failure analysis of composite structures. Cusps are characteristically associated with mode II fractures[4,8–19] but are only found in relatively brittle systems since they are formed from microcrack nucleation ahead of the crack tip.[8,19] The tilt of the cusp can either be in the direction of crack propagation or in the opposite direction.[4,8,20] There is some evidence to suggest that the angle at which the cusps are orientated to the fracture plane is related to the amount of mode II loading.[11,14,15,21,22] In epoxy matrix systems, as in the present work, the amount of fibre pull-out is greater in mode I than in mode II.[18] Clean fibres have been identified on both brittle mode I[15] and tough mode II[11] fracture surfaces; however, fibre/matrix adhesion is related to interfacial strengths and clean fibres cannot be used with certainty to distinguish between mode I and mode II fracture surfaces.

In certain epoxy-resin systems, such as 914 matrix composites (from Ciba Composites, UK), the presence of second-phase plasticizing agents, e.g. PES, blunts the appearance of all fracture features. Figure 1 highlights the basic features of T300/914 with nodules of PES embedded within the epoxy matrix and surrounding the carbon fibres.[23] This has the effect of rendering river markings, feathering, shear cusps, etc., indistinct, unlike in more brittle matrices where it is considerably easier to identify directions of damage growth. This problem is compounded in fatigue specimens when the fretting of opposing damage surfaces rounds off sharp fracture features. For these reasons it can be quite difficult to establish initiation sites and directions of growth in complex structural components unless the fractographic data is interpreted in the light of known failure details of actual tests.

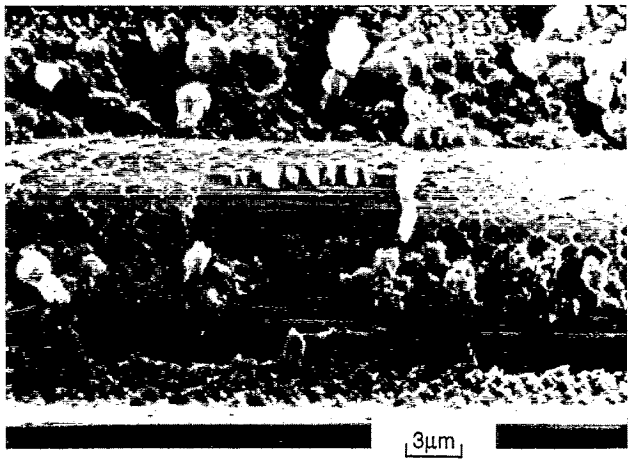

Fig. 1. Microstructure of carbon/epoxy T300/914 shows a thin coating of epoxy matrix adhering to a fibre. Small nodules (≈1 μm in diameter) of poly(ether sulphone) are embedded in the bulk epoxy matrix material. (From Lowe[26].)

Six carbon-fibre/thermoplastic I-beams (made from carbon-fibre (AS4)/PEEK, carbon-fibre (T300)/PEEK and carbon-fibre (T300)/PES), loaded to failure in three-point bending, were evaluated by Greenhalgh.[24] Different layups and manufacturing methods were used for most of the beams. To promote web failure, carbon-fibre/epoxy caps were included on five of the beams. The web of the beams had only +45°/−45° plies for resistance to shear stresses while the flanges were made of unidirectional plies to withstand bending. Several different failure initiation sites were found: through-thickness failure of the compression flange (the one beam without a reinforcing cap), shear failure in the web, delamination of the tensile flanges due to fibre waviness and delamination of both flanges due to poor consolidation. A variety of failure strains was observed due to different defects caused by the manufacturing methods. Fibre waviness was detected on a few fracture surfaces, both in-plane and out-of-plane. Fibre waviness arises during fabrication either (i) because of incorrect cooling rates, which can lead to some regions of a component cooling more rapidly than others and, consequently, inducing differential thermal stresses, or (ii) because of movement or distortion of the structure when the temperature of the laminate is above the glass transition temperature, T_g, of the matrix. Poor consolidation, on the other hand, can be caused by insufficient pressure or by the introduction of volatile materials between plies during fabrication.

T300/914 carbon-fibre/epoxy beams, representing a thick walled wing spar section, were tested in shear by Gamziukas.[25] The spar web consisted of a $[\pm 45°/(\pm 45°/90°_2)_2/\pm 45°_2/0°_2]_s$ laminate lay-up and contained an off-centre drop-shaped semi-symmetrical cutout. The load versus shear strain curve was seen to be linear up to very high loads. No buckling could be seen on any of four specimens. Extensive tensile damage in all the beams extended along a +45° line from each end of the cutout. This damage continued as a shear failure in opposite directions along the top and bottom of the web/flange interface. The +45° tensile failure was limited to the ±45° plies, with fibre failure in the −45° plies and matrix failure parallel to the fibres in the +45° plies. The 0° and 90° plies experienced matrix dominated failure parallel to the fibres along 0° and 90° lines originating from, for all plies, the common failure initiation area. Compressive damage extended from each end of the cutout along a −45° line and ended close to the flange; this was not as extensive as the tensile damage. Extensive delamination existed between plies of different orientation. It was not possible to establish from a

fractographic examination of the beams whether the tensile or compressive damage was the critical event which led to failure. Hollman[26] used finite element analysis to determine the stress conditions in these same beams[25] but could not determine the critical failure mode.

Purslow[3] determined the failure process of an I-beam made from XAS carbon-fibre in a 914 epoxy matrix which had failed statically in three-point bending. Interlaminar shear of the compression cap at 0°/45° ply interfaces was the first failure and was initiated by an in-plane shear failure of a 0° ply. Delamination at a +45°/−45° ply interface was also observed and this fracture surface was seen to have a rougher texture than the other delaminated surfaces. Post failure abrasion of mating surfaces had been present, resulting in dull surfaces covered with debris. Peel fracture was only observed at a single ply interface in the flange during the whole failure process. The tensile stresses causing the peel damage were induced by buckling of the compression flange. After the compression flange was severely weakened, failure occurred in the web by in-plane stresses. The tension cap underwent gross deformation but did not fracture until the web finally failed.

With regard to the present paper, the authors have only examined the fracture surfaces of I-beams, see Figs 2–5; the fractography of associated fracture mechanics coupons are discussed elsewhere.[21] Both unnotched and notched carbon/epoxy and E-glass/epoxy beams have been tested to failure and this paper describes the failure processes which occur within the four types of I-beams. Within the fillet regions of the beams, i.e. between the web/flange junctions, are strips of wound prepreg tow and unreinforced resin. These regions of pure cured resin are visible to the naked eye (of the order of millimetres in size) after failure or sectioning of a beam. This unreinforced resin, presumed to exist because of imperfect consolidation of the beams, is convenient for microscopic observation. Similarly, at higher magnifications it is possible to examine resin between fibres in the web and flange regions of the beams and it is such regions that provide most information about the manner of fracture within that general region of a particular I-beam. The component geometry and testing configuration are outlined below together with the main fractographic techniques which have been used. The paper discusses the various fracture features which have been identified in statically tested I-beams and this information is interpreted in the light of observed beam behaviour during testing to establish the regions of damage initiation and the subsequent directions of damage evolution. Damage that was observed within fatigue tested I-beams is to be discussed in a subsequent publication.[27]

2 EXPERIMENTAL

The testing arrangement has been described in greater detail elsewhere[28] and consequently only a summary is given of the salient points that are of immediate interest in this particular paper. All I-beams have been manufactured using two preformed C-sections and two flange caps all of which were cured together in the same autoclave operation. The I-beams were of length 1200 mm, web depth 125 mm, flange width 75 mm and thickness 3 mm, as shown in Fig. 2. A 3 mm fillet radius was used at the web/flange junction; two spirally wound prepreg ropes (tows) were used to fill the triangular void which exists in this junction.

The stacking sequence was the same in the web and flanges of all the I-beams and contained a balanced, antisymmetric combination of +45°, 0° and −45° plies, where the 0° direction is defined to be along the axis of the beam. Commercially available software[29] was used to design the beam stacking sequence such that there was a minimum number of coupling terms in the laminate stiffness matrix as well as the lowest possible interface moment, i.e. the τ_{zx} and σ_z stresses through the I-beam thickness were minimised. The actual stacking sequence which was used is $(-45°/0°/+45°)_{2s}(+45°/0°/-45°)_{2s}$, i.e.

$$-45°/0°/45°/-45°/0°/45°/45°/0°/-45°/45°/0°/$$
$$-45°/45°/0°/-45°/45°/0°/-45°/$$
$$-45°/0°/45°/-45°/0°/45°$$

The mechanical properties of the carbon-fibre/epoxy, T300H/914, and glass-fibre/epoxy, E-

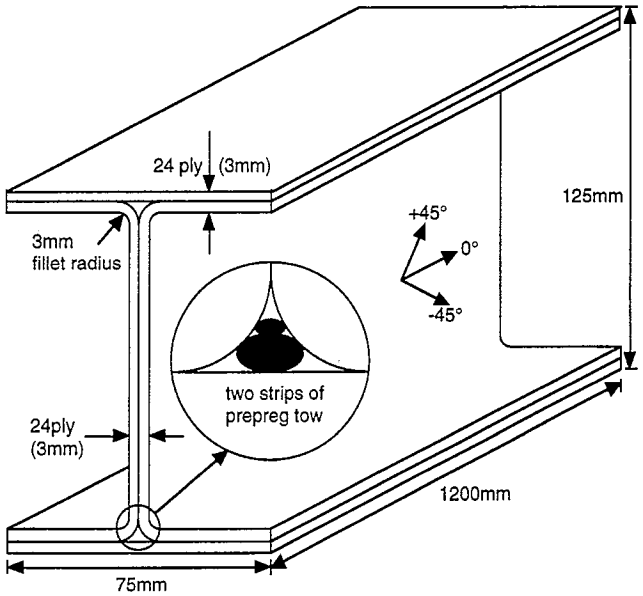

Fig. 2. Carbon/epoxy (T300/914) and E-glass/epoxy I-beams are manufactured using two channel sections, two flange caps and strips of wound unidirectional prepreg tow. The 24-ply stacking sequence is $(-45°/0°/+45°)_{2s}(+45°/0°/-45°)_{2s}$.

glass/914, material systems were measured in accordance with the CRAG guidelines[30] and are given in Table 1. This table details both the unidirectional properties as well as those corresponding to the multidirectional stacking sequence that was used to manufacture the I-beams.

A four-point bending configuration was used with an arrangement of eight loading pads which were adhesively bonded to the web and undersides of the flanges as shown schematically in Fig. 3. Position control on a servohydraulic machine was used for all static tests. One of each of the carbon/epoxy and glass/epoxy beams were statically tested in the virgin unnotched state; two identical beams had notches machined in the web and flange regions. The notches consisted of two circular holes, of diameter 46 and 60 mm (some 40 and 50% of the internal web depth) located centrally in the two web regions between the sets of outer loading pads where the shear is constant and a maximum. A longitudinal array of six 5 mm diameter holes was also machined in both the tensile and compressive flanges of the web-notched beams, adjacent to the mid-length of the beams. No damage was evident around these latter holes and consequently they are not discussed any further in this particular paper. Whilst further details are provided elsewhere,[28] Table 2 summarises the configurations of the various beams that have been tested under static load conditions.

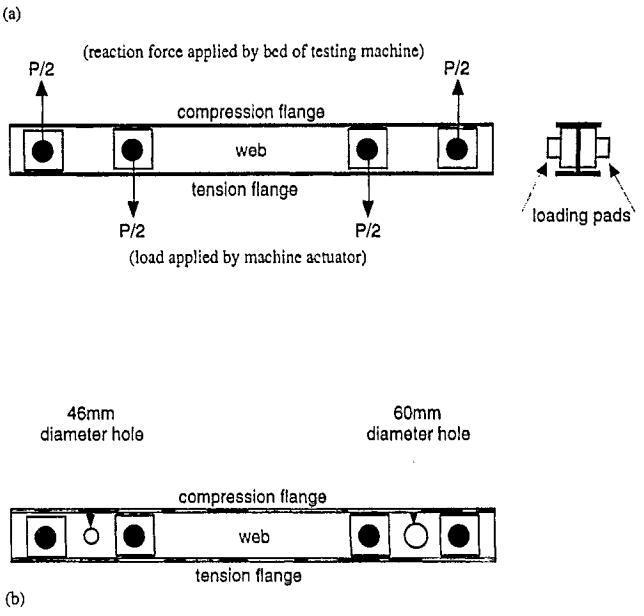

Fig. 3. Schematic representation of the four-point flexure loading arrangement used for static testing of (a) unnotched I-beams and (b) notched I-beams. Static tests have been under a displacement mode of control.

3 DAMAGE DETECTION TECHNIQUES

3.1 Ultrasonic scanning

Ultrasonic C-scanning has identified the extent of delamination damage in the I-beams. It was also possible to determine between which plies the various delaminations were present by consideration of the A-scans associated with a particular position on the beams. The presence of damage associated with other mechanisms such as matrix cracking, splitting, and fibre fracture could only be identified when they were present in sufficient density to attenuate the ultrasonic signal. Damage mechanisms other than delamination can be identified[31] by spectral analysis of ultrasonic signals. However, this has not been attempted within this particular programme; rather, it is the combined use of different techniques that have been used to quantify the different mechanisms of damage that exist throughout the I-beams.

3.2 X-radiography

Dibromomethane and zinc iodide were used as dye-penetrants when X-raying the carbon/epoxy and E-glass/epoxy components after fracture. Specimens

Table 1. Measured mechanical properties of unidirectional and multidirectional carbon/epoxy (T300H/914) and glass/epoxy (E-glass/914) Ciba Geigy materials

Property	T300/914		E-glass/914	
	Unidirectional	Multidirectional	Unidirectional	Multidirectional
E_{11} (GPa)	134·75	54·75	45·37	26·68
E_{22} (GPa)	8·24	21·98	15·20	16·94
ν_{12}	0·325	0·704	0·289	0·477
ν_{21}	0·012	0·287	0·074	0·291
X_{Lten} (MPa)	1563·00	534·20	1049·00	432·77
X_{Tten} (MPa)	44·76	277·12	46·48	220·45
G_{12} (GPa)	Not measured	—	6·03	—

The stacking sequence used for the multidirectional laminates was the same as that used to manufacture the I-beams, namely $(-45°/0°/45°)_{2s}(45°/0°/-45°)_{2s}$. Note that no shear modulus has been measured for the multidirectional stacking sequence: this is in agreement with the CRAG guidelines.[30]

were soaked in dye-penetrant for a matter of hours to promote ingress into all cracks; excess dye-penetrant was removed prior to X-raying the specimens. Use of the zinc iodide provided greater resolution of the damage than dibromomethane although, since the zinc iodide was based on a saline solution, it deposited a saline residue on the fracture surface. This residue tended to mask many important fractographic features and, consequently, dibromomethane was used when it was also necessary to examine the fracture surface of a particular component using optical microscopy. Isopropanol was used to remove the dibromomethane after radiography, and before potting the specimens for subsequent polishing and optical microscopy, since the dye-penetrant tended to leach out of the composite specimens and inhibit the curing of the potting compound. For X-raying the carbon/epoxy components, a voltage of 20 kV at 3 mA for 5 min at a distance of 0·3 m was appropriate, whilst approximately double this voltage was more suitable for the E-glass/epoxy material.

3.3 Optical microscopy

Both optical and stereo optical microscopy have been used. It has proven more convenient to use an optical microscope when identifying matrix cracking and delaminations within polished section specimens, whilst the greater depth of field which is available on a stereo optical microscope is more appropriate for examining the fracture surfaces of broken specimens. Magnification factors from 50× to 400× are available on the optical microscope, although 50× and 100× factors are usually sufficient to identify delaminations, matrix cracks and the wound prepreg tow laid within the fillet region of the beams. The stereo optical microscope can typically magnify from 10× to 200× and as such is complementary to the SEM. The depth of field available on the stereo optical microscope means that fracture marks on the neat resin in the fillet regions of the I-beams can usually be kept in focus, which is necessary when trying to identify growth directions across the resin. Directions of damage development can often be successfully identified with the stereo optical microscope alone without recourse to the SEM.[3] The stereo optical microscope is especially useful for quickly examining large areas of fracture surface and for identifying particular areas that merit further examination with the SEM. The time required for specimen preparation and limitations on working areas (and consequently specimen size) within the vacuum chamber of the SEM means that the stereo optical microscope is used whenever possible. The SEM is mainly used to provide greater depth of field and resolution of specimen fracture surfaces (possibly to identify cusp angles and consequently ratios of mode mixity).

3.4 Scanning electron microscopy

A JEOL JSM-5300 scanning electron microscope was used throughout this work. The time required to set up the SEM can be almost one hour (time for gold sputtering and mounting a specimen as well as evacuation of the SEM vacuum chamber) and examining the fracture features of any specimen satisfactorily usually takes a few hours. This, and the limited space of the chamber, which could not accommodate specimens larger than 2 in × 2 in, means that the SEM was only used when sufficient clarity could not be obtained using optical microscopy. Experience with the SEM is necessary in order to obtain the maximum information possible concerning the fracture of any specimen. Since greater depths of field and magnification factors are available on the SEM than on a stereo optical microscope, it is usually easier to identify river markings, feathering, shear cusps etc.; this is especially so when examining plain resin which has quite sharp out-of-plane three-dimensional features. However, inexperience in using the SEM, particularly setting the stigmator, charging voltage, filament spot-size and focusing can make it difficult to obtain clear images (low graininess in texture and good contrast) of such fracture features. It is important that the charging voltage is not set too high (i.e. 10–15 kV is reasonable for 914 resin) otherwise the resin fragments, which record the vital fracture patterns, can charge and be destroyed, despite having been sputter coated.

4 OVERALL FAILURE MODE OF I-BEAMS

The loads and initiation sites associated with static failure of the unnotched and notched beams have already been summarised in Table 2. Figure 4 shows flange deformation prior to fracture and damage after fracture in an unnotched I-beam. The latter is also presented schematically in Fig. 5. Static failure of the unnotched beams was due to local buckling of the compression flange. Delamination initiated from the edge of the flange at a point which coincided with the crest of a buckle (see Figs 4 and 5) and, having propagated to the fillet region, advanced through the web and towards the tensile flange of the beam.[28] The position, mode and dimensions of the buckling with respect to the flange, web and loading pads are given in greater detail in the first paper of this series.[28]

Failure of the notched beams, on the other hand, was due to matrix cracking, under local tensile stresses, which initiated around the boundary of the large web-notches and advanced primarily towards the tensile flange but also towards the compressive flange.[28] The visual evidence of tensile damage is seen in Fig. 6 as a relatively clean fracture from the hole edge towards the tension flange of the carbon/epoxy beam and as a generally jagged fracture from the hole

Table 2. Summary of static test conditions of the carbon/epoxy and glass/epoxy I-beams

Geometry	Carbon/epoxy		Glass/epoxy	
	Unnotched	Notched	Unnotched	Notched
Failure load	96 kN	74 kN	74·8 kN	57 kN
Failure initiation site	Buckling in compression flange	Web cutout	Buckling in compression flange	Web cutout

edge toward both the tension and compression flanges of the glass/epoxy beam. Fibre fracture, splitting and delamination were also present at failure in the notched beams.

The following sections identify and discuss the location and presence of the different damage mechanisms (i.e. matrix cracking, splitting, fibre fracture and delamination) that were detected using the ultrasonic, radiographic and microscopic techniques in both the unnotched and the notched I-beams.

5 FRACTOGRAPHY

5.1 Unnotched I-beams

The appearance of damage within the carbon/epoxy and glass/epoxy beams is visually similar, with damage being present in the same general areas of the compression flange and the web of the two beams. A greater extent of damage is, however, present in the carbon/epoxy beam. For example, the damage in the web of the glass/epoxy beam did not extend as far as the tension flange. Consequently, it is damage associated with the carbon/epoxy beam that has been examined in greater detail, and which is discussed in this section.

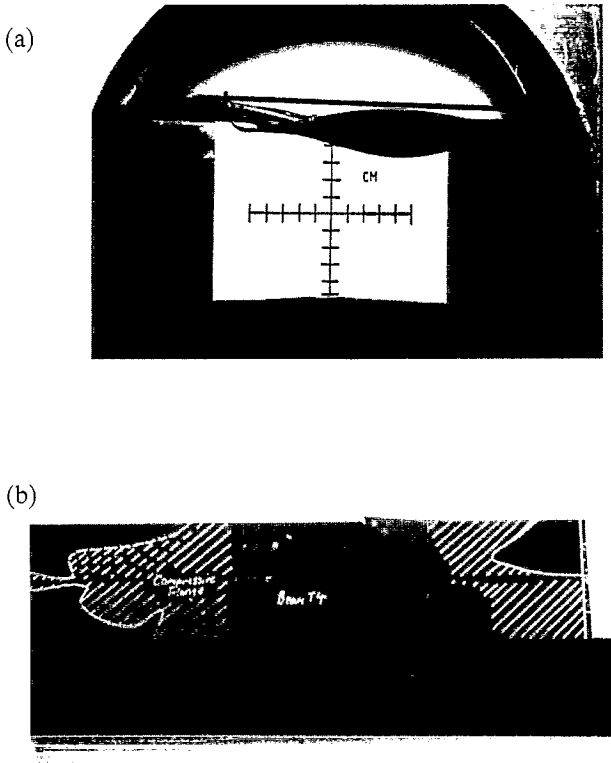

Fig. 4. Unnotched I-beam: (a) side view taken immediately before failure, and (b) plan view taken after failure.

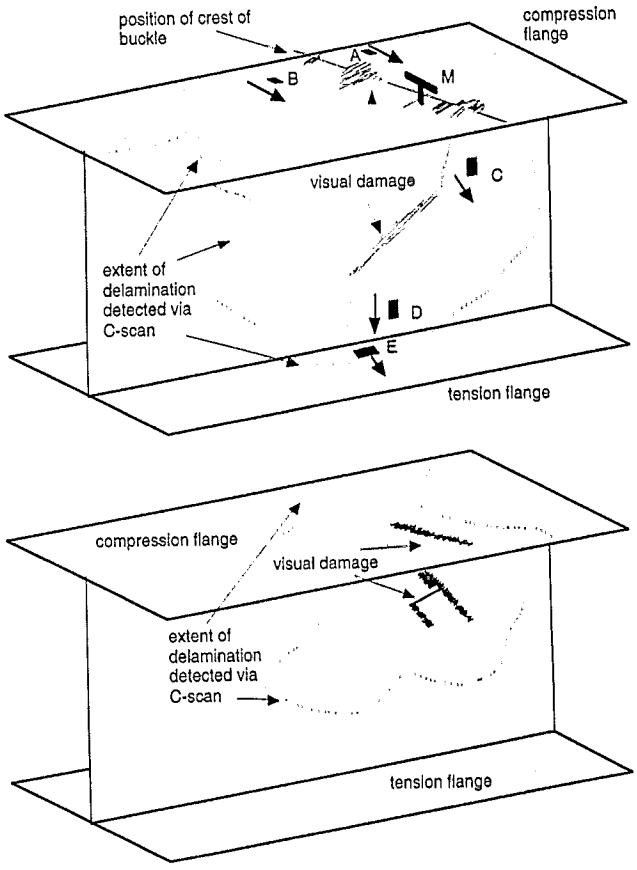

Fig. 5. Schematic representation of the damage, failure sequences, and locations of microscopy sections in (a) the unnotched carbon/epoxy I-beam and (b) the unnotched glass/epoxy I-beam. This region of I-beam is between the central pairs of loading pads; no damage exists outside this region, see Fig. 3(a). The first paper in this series[28] provides details of the visual appearance of the general damage. Sections A and B (see Figs 7 and 9) are from the compression flange; section M (see Fig. 10) from the compression flange/web junction; sections C and D (see Figs 12–14) from the web region; and section E (see Fig. 15) from the tension flange. (Total flange width is 75 mm; internal web depth is 119 mm.)

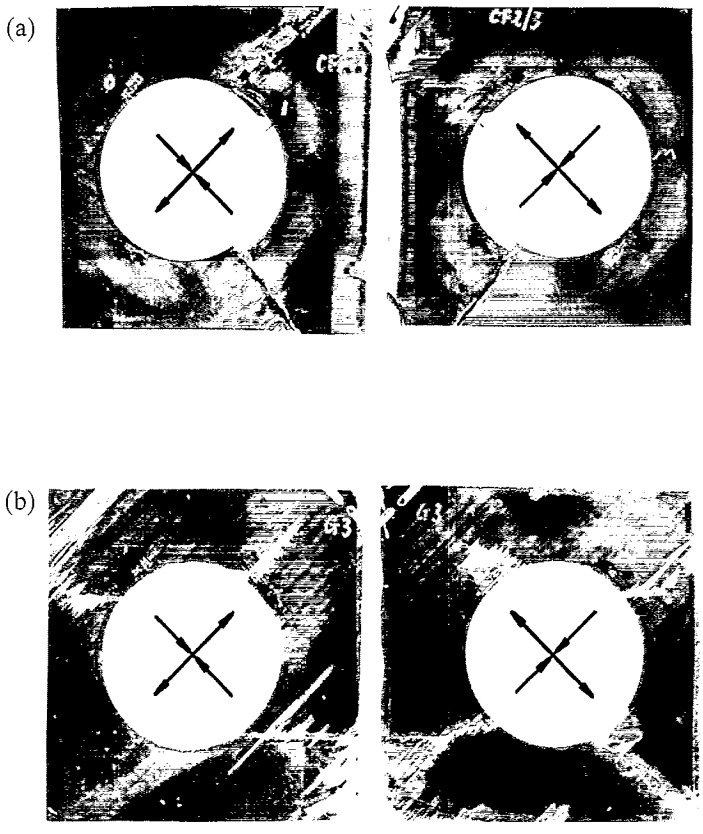

Fig. 6. Visually identified damage around the front and back of shear-loaded web cutouts (60 mm diameter) in (a) the notched carbon/epoxy I-beam and (b) the notched E-glass/epoxy I-beam. In all cases, the compression flange is along the top of the photographs and the tension flange along the bottom. The local directions of resolved tensile and compressive stresses are indicated.

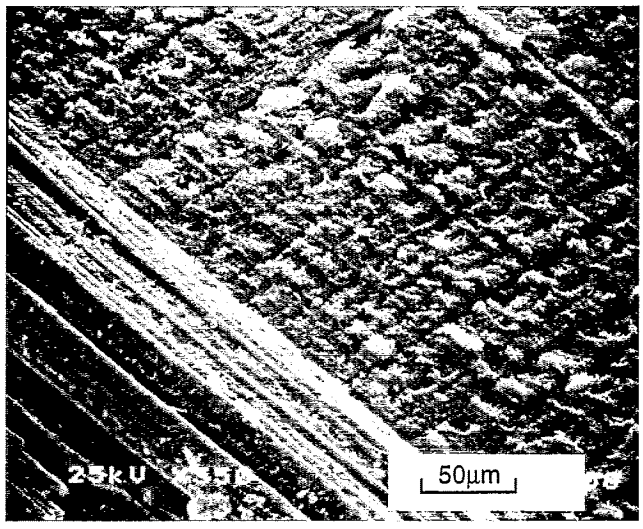

Fig. 7. The fracture surface of section A (see Fig. 5) shows fibre bundle pull-out and some fibre fracture (bottom left-hand corner of micrograph) and flat featureless resin fracture (upper right-hand half of micrograph). The picture was taken close to the edge of the flange where the zone of fibre pull-out changes into the flat featureless zone of resin fracture. This corresponds to a change of mode I to mixed mode fracture. The local growth direction within the micrograph is from left to right; this corresponds to damage propagating from the flange free edge towards the fillet region. (Tilt angle is 45°.)

5.1.1 Compression flange

The visible damage within the compression flanges of the carbon/epoxy and glass/epoxy beams is shown in Fig. 4 and schematically in Fig. 5. In both beams the damage extends across the complete width of the flange and the extent of delamination, as detected using ultrasonic C-scanning, has been highlighted. The different samples that were cut out for fractographic examination are identified as locations A and B in Fig. 5. The arrows shown indicate the direction of crack propagation, which is from left to right in the various micrographs, unless otherwise stated.

The main delamination, i.e. that along the +45°/−45° ply interface of the flange mid-thickness, was examined using the SEM at regions A and B of the carbon/epoxy beam, shown in Fig. 5. A preliminary visual examination of the delamination surfaces identified 'tide' markings (not shown in the figures) which initiated from the flange edge at a point which corresponded to a crest on the flange buckle. This observation is supported by the fractographic analysis which identifies a highly mode I (i.e. tensile-opening stress) dominated fracture region[11,18,21,23,32] close to the edges of the flange (region A). This mode I fracture appearance, as typically shown in Fig. 7, has some fibre pull-out (seen

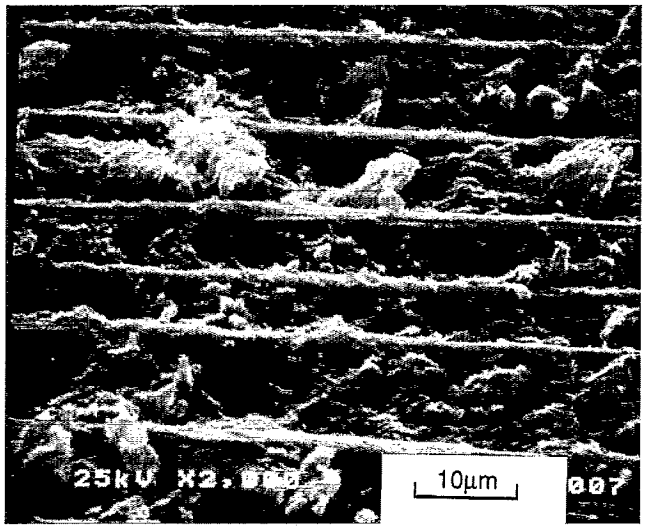

Fig. 8. Evidence of mode II dominated mixed mode fracture which was typically observed on the compression flange away from the flange free edge. Cusps (≈5–10 μm in size), oriented at a high angle to the plane of fracture (≈40°), can be seen spaced between fibres which are relatively clean of matrix material. The local direction of growth within this micrograph is from left to right. This corresponds to a global direction of damage growth that is from the flange edge toward the centre of the flange. (Tilt angle is 65°.)

as fibre bundles here) and relatively flat, featureless resin. Some cusps were found in the resin elsewhere on the compression flange, further away from the main fracture, as shown in Fig. 8. The orientation angle of these cusps to the plane tends to be high (≈40°), which suggests a mode II (i.e. shear) dominated mixed-mode fracture.[11,15,21,22] This evidence for mode II dominated fracture away from the flange edge is supported by the relatively clean fibres and the rough resin. Also, from studies on the fracture toughness specimens of the same material and stacking sequence,[21] if the cusps were oriented normal to the fracture direction, then they would indicate a fracture direction that is from the flange edge towards the centre of the flange.

The fracture plane shown in Fig. 9 for region B propagated along two interfaces (+45°/0° and −45°/0°). Propagation transversely through the 0° ply appears to have been less energetically favourable as the crack continued along the outer 45°/0° ply interface. Some small cusps can be seen in the top right-hand corner of the micrograph which indicate that a mode II loading component has been associated with fracture along this interface.

It is concluded, therefore, that delamination in the compression flange initiated from the crest of a buckle at the edge of the flange due to predominantly mode I (tensile) stresses. Subsequent delamination was towards the fillet region and along the length of the compression flange in a mixed mode manner. In some regions of the flange, especially away from the initial delamination damage, the mixed mode fracture was dominated by mode II conditions, i.e. shear loading conditions.

5.1.2 Compression flange/web junction

A polished through-thickness section, identified by section M in Fig. 5, was taken at the flange/web intersection, i.e. at the fillet region, specifically to identify the principal delaminations and the presence of other damage in the curved sections of the beam. Figure 10 presents a schematic representation of the various delaminations and matrix cracks which were observed at the flange/web intersection: the major delamination between the C-section and the prepreg tow is evident, as are further delaminations between −45°/0°, +45°/0° and +45°/−45° plies, and matrix cracking within individual plies and also between different inter-ply delaminations. It is worth noting that these damage mechanisms are also present in composite tubes that have been subjected to axial crushing.[33–36] The extent to which matrix cracking,

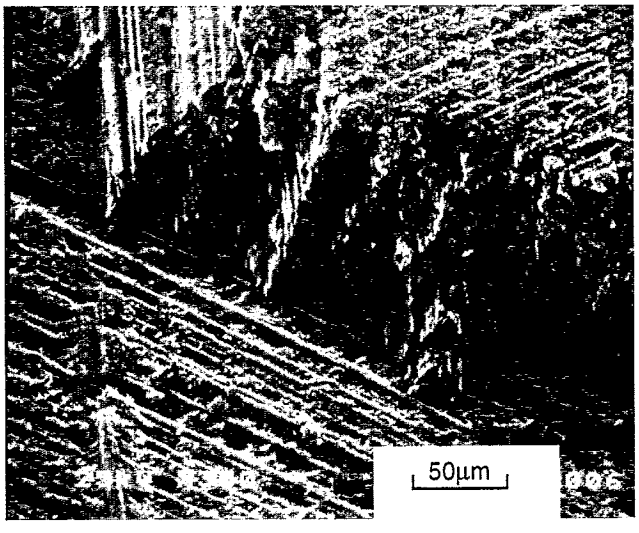

Fig. 9. Fracture surface of section B (see Fig. 5) shows delamination growth which occured along two different interfaces, i.e. the main crack jumped through a ply. Delamination was through +45°/0° (bottom left-hand corner of micrograph) and 0°/−45° (upper right-hand corner of micrograph) ply interfaces. Cusps can be seen on the fracture surface in the top right-hand corner of the micrograph but not clearly at this low magnification. This delamination along two interfaces was accompanied by matrix cracking and fibre fracture of the 0° ply. The local growth direction is from left to right in this micrograph. (Tilt angle is 65°.)

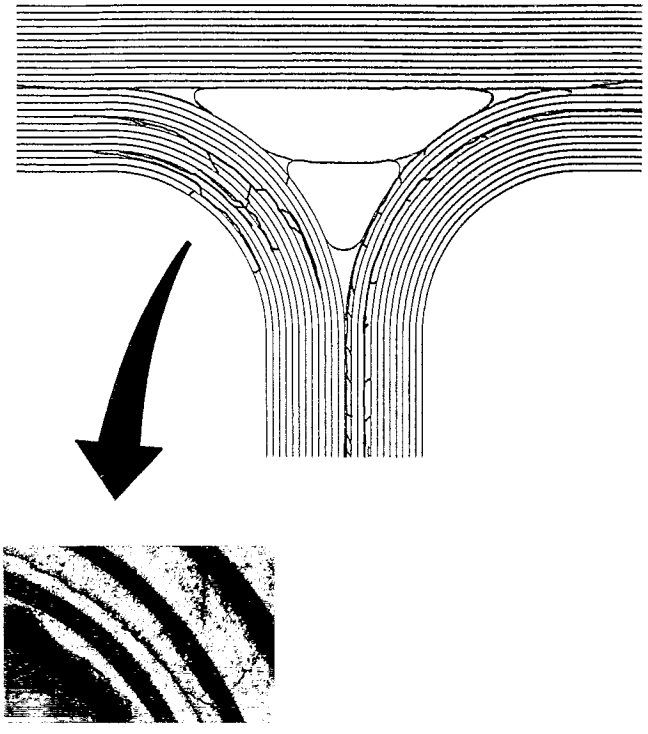

Fig. 10. Schematic representation of damage in the fillet region of the compressive flange of the unnotched carbon/epoxy I-beam (see section M of Fig. 5). Damage consists principally of delamination between the backs of the channel sections, between the channel sections and the flange cap and various 0°/45° and +45°/−45° ply interfaces. Matrix cracking of plies in the curved fillet region had also occured (see text). Each ply has a nominal thickness of 0·125 mm.

delamination, splitting, etc., occur as energy absorption mechanisms in a composite structure depends on geometry, boundary and loading conditions and material characteristics.

As can be seen in Fig. 10, principal delaminations lie generally between the backs of the two C-sections and the flange cap and the C-sections, i.e. along the +45°/−45° interfaces. Delaminations, however, are not confined to interfaces of 90° relative angle: they are also to be seen along −45°/0° and +45°/0° interfaces but not between +45°/+45° or −45°/−45° interfaces, where the relative angle is 0°. It appeared as though the two pieces of tow became separated from the adjacent plies with cracks usually being present in the resin rich areas, which exist at the three corners of the fillet, and extending to the extremes of the polished sections. Taken alone, this information would not indicate whether the delaminations started in the fillet region and propagated towards the edges of the flange and along the web, or vice versa. However, it has already been established in the previous section that delaminations propagated from the flange edges towards the fillet region.

The wound prepreg material in the fillet region (see Fig. 2) is surrounded by plain resin which fractures in a brittle manner as shown in Fig. 11. The river markings in the resin shown in Fig. 11 indicate a direction of crack propagation that is from the fibres in the flange (left of Fig. 11) into the resin rich area at the fillet (right of Fig. 11).[1,4,8,17] This fractographic evidence also supports the direction of damage propagation identified in Section 5.1.1, namely from the flange edge towards the fillet region.

5.1.3 Web

Samples C and D were cut from the fractured web as shown in Fig. 5. Subscripts I and II denote two samples at the same location but on opposite surfaces of the delamination, whilst the arrows shown indicate the direction of crack propagation, which is from left to right in the various micrographs unless otherwise stated. During testing, damage was seen to propagate from the buckled compression flange into the web and through to the tension flange.

Figure 12 shows the fracture surface of sample C, which is close to where the failure entered the web from the compression flange. The delamination propagated along the +45°/−45° interface between the backs of the channel sections. There were frequent cracks into the adjacent plies and there were also many ridge and valley formations corresponding to the presence of shear stresses. The few cusps that were formed due to the action of the shear stresses were small and oriented at approximately 45° to the fracture surface. Some debris and nodules could be seen, although very few fibre ends were found. Consequently, no clear indication of the failure direction could be established by examining the resin. It is suggested that this was a mixed mode of failure with about equal mode I and II components.[11,21,22,37]

The appearance of the fracture surface near the

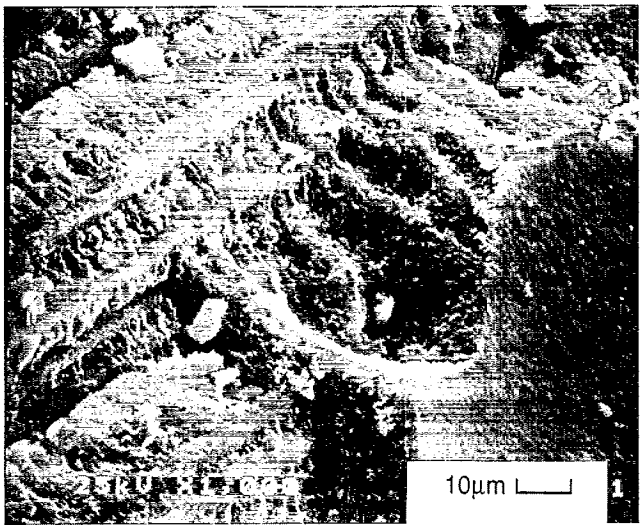

Fig. 11. Zones of resin richness and voids have been seen (bottom right-hand half of micrograph) close to the junction of the compression flange and the web of the carbon/epoxy I-beam. The river markings, seen in the middle area of micrograph, indicate the direction of fracture as being from the fibres of the flange into the resin of the fillet (top left to bottom right). (Tilt angle is 35°.)

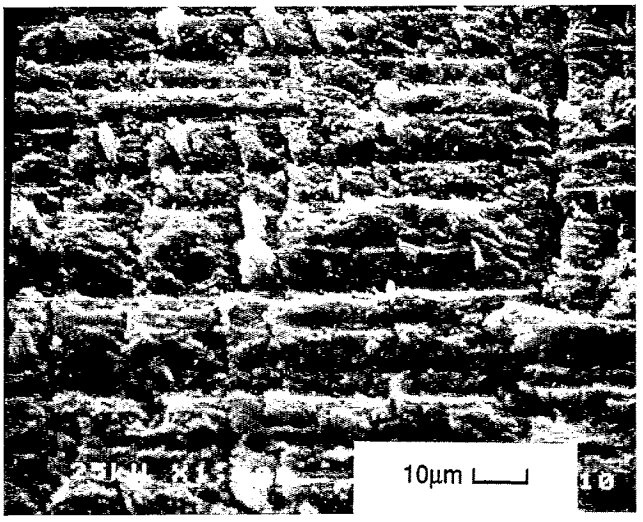

Fig. 12. Resin fracture surface of section C, which is towards the centre of the web of the unnotched carbon/epoxy I-beam (see Fig. 5), is relatively flat. Frequent matrix cracks to the underlying ply (seen typically running top–bottom in the right edge of the micrograph) and some valleys in the matrix (irrgeularly spaced and oriented left–right in the micrograph) are seen. Small cusps are also present throughout the matrix (at ≈45° to the fracture plane) and the apppearance of this fracture surface corresponds to a mixed mode of failure with approximately equal components of mode I and mode II. (Tilt angle is 55°.)

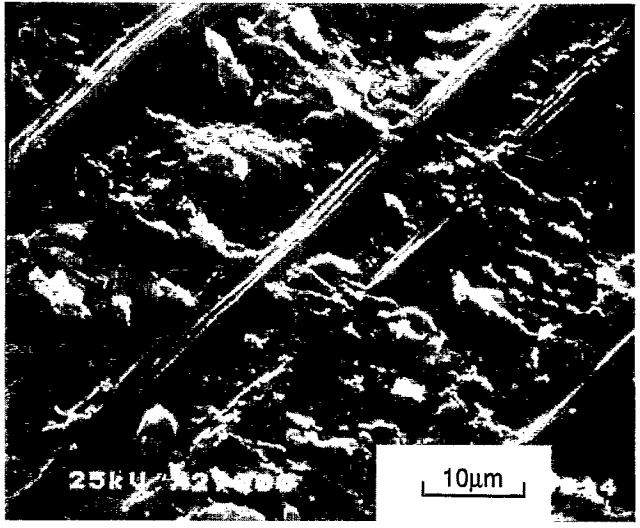

Fig. 13. Section D_I (see Fig. 5), taken from the web region of the unnotched carbon/epoxy I-beam, is the mating surface of section D_{II} (see Fig. 14). Very clean fibres, sparce resin and rough resin fracture between the fibres, and resin cusps oriented at a large angle (≈66°) to the fracture plane are evident. This suggests a highly mode II dominated fracture. Resin rivers can be seen propagating from a fibre into the resin (indicated by arrow). The fact that this particular fracture surface is sparse of resin implies that the opposite fracture surface (see Fig. 14) should be resin rich with many fibre imprints: this is indeed the case. The local growth direction in the micrograph is from left to right. (Tilt angle is 40°.)

tension flange indicates that the failure of this region of the web is mode II dominated.[1,4,22,38] Figure 13 shows the typical morphology of sample D_I having a thin, but rough, resin fracture including distorted

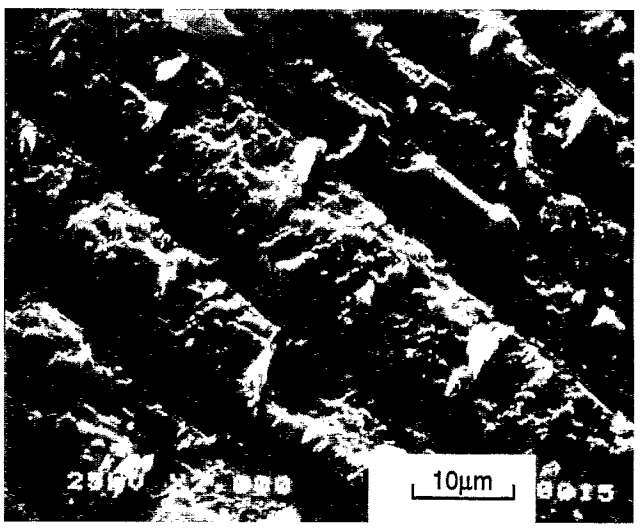

Fig. 14. Section D_{II} (see Fig. 5), taken from the web region of the unnotched carbon/epoxy I-beam, is the mating surface of section D_I (see Fig. 13). The fact that this particular fracture surface is resin rich implies that the opposite fracture surface (see Fig. 13) should be sparse of resin: this is indeed the case. The local growth direction in the micrograph is from left to right. (Tilt angle is 40°.)

cusps and very clean fibres. Upon close inspection, resin rivers can be seen to propagate from the fibres into the resin between the fibres (indicated by the arrow). Again, due to the small amount of resin, the delamination obviously propagated close to this ply of the +45°/−45° interface. Consequently, the mating fracture surface, i.e. sample D_{II}, should be resin rich with a lot of fibre imprints and this is indeed the case, as seen in Fig. 14. Many valleys and fibre imprints, corresponding to the clean fibres on the surface of sample D_I, can be seen. Very few fibre breaks are seen on the surface. The large average cusp angle (66°) and the clean fibres in Fig. 13 imply crack propagation has occurred under a relatively high mode II loading component.[8,15,17] Less debris and fewer nodules were observed in this region close to the tension flange than had been observed close to the compression flange; this implies that less abrasion and movement of the fracture surfaces occurred here. This corresponds directly with what actually happened during testing, namely the damage propagated from the compression region of the web towards the tension flange. Thus, the amount of gross deformation and fracture was greater in the compression region of the web than in the tension region.

Consequently, it is suggested that delamination damage along the +45°/−45° midplane interface of the backs of the channel sections of the web occurred under a mixed mode loading. As the delamination propagated initially from the region close to the compression flange, this fracture was approximately equally mode I and mode II but as the delamination reached the tension flange the fracture became predominantly mode II. It is necessary to use numerical techniques, such as those used in paper four of this series,[39] to predict the mode I and II components of loading through the web midplane since it is not intuitively clear whether fracture should be due to mode I or mode II conditions. It is possible, however, that a greater amount of mode II loading was present at the crack tip because of imperfect symmetry of both loading and damage along the axis of the I-beam. This lack of symmetry could be due to different amounts of damage in the two channel sections and any slight misalignments in the bearings and loading pads of the I-beam.

5.1.4 Tension flange

The extent of damage in the tension flange has also been examined using ultrasonic C-scanning, optical and electron microscopy. No damage was identified in the tension flange of the glass/epoxy I-beam; the only damage that was seen was in the carbon/epoxy I-beam. Within the carbon/epoxy beam, the surface of the tensile flange retained its integrity when the damage propagated from the web region to the tensile flange. The damage that was present in a through-

thickness microscopy section (i.e. in a section similar to that shown for the compression flange in Fig. 10) identified the largest delamination to be between the backs of the C-sections, and between the C-sections and the flange cap. In all cases these were +45°/−45° ply interfaces. Secondary delaminations existed between other +45°/−45° interfaces and 0°/45° interfaces. In addition to these delaminations, matrix cracking also occurred in all plies, especially in the region of curvature of the fillet region.

The delamination fracture surface between the flange cap and the channel regions of the tensile flange was examined using SEM. Fibre pull-out, characteristic of mode I dominated fracture, is found close to the fillet region of the tension flange (not shown), whereas a flat featureless +45°/−45° delamination surface, shown in Fig. 15, is identified further away from the fillet region. The morphology of this region away from the fillet, shown in Fig. 15, resembles a mixed mode failure having approximately equal mode I and II components.[11,21,22]

In conclusion, therefore, it has been observed that damage propagated from the web of the carbon/epoxy I-beam towards the tension flange/web junction and thence outwards towards, but not reaching, the edge of the tension flange. This damage was principally in the form of delamination between the +45°/−45° midplane interface and was highly mode I close to the fillet region. As the delamination propagated away from the fillet region, this was in a mixed mode manner with approximately equal components of mode I and mode II.

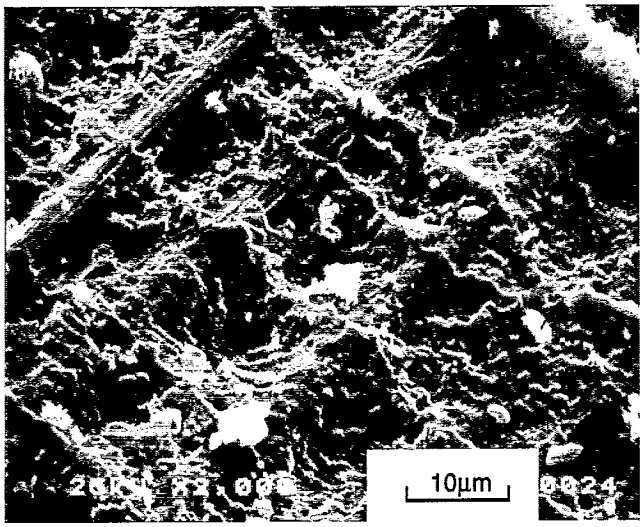

Fig. 15. The morphology of the fracture surface (section E of Fig. 5) of the tensile flange, some distance away from the flange/web junction, is relatively flat, with fibres being clearly coated in resin. This is characteristic of a mixed mode fracture having approximately equal components of mode I and mode II. The local direction of growth is from left to right; this corresponds to growth from the web/flange junction toward the flange free edge. (Tilt angle is 40°.)

5.1.5 Summary

The failure sequence of the unnotched I-beams can be summarised as having initiated from an edge delamination at the crest of a buckle on the compression flange. This initial damage was predominantly due to mode I (tensile) stresses, and was along the mid-thickness of the flange, i.e. the interface between the flange cap and the channel section. Damage subsequently advanced, in a mixed mode manner, towards the flange/web junction and along the length of the compression flange. Delamination through the web region, towards the tension flange, was initially in a mixed mode manner but changed to a highly mode II fracture. This change in loading mode, to an essentially shear fracture between the backs of the channel sections, was most likely due to changes in the state of stress at the delamination front when the distribution of load and damage became increasingly non-symmetric along the axis of the I-beams (i.e. in the two channel sections). Delamination damage also propagated from the junction of the web and tension flange out towards the free edge of the tension flange. However, a displacement mode of control was used during testing, and because the load was removed from the I-beam immediately upon fracture of the compression flange, there was no visual evidence of damage in the tension flange.

Thus, the principal and predominant damage mechanism in the unnotched I-beams was delamination occurring at the crest of a buckle on the compression flange and this led to catastrophic fracture which was accompanied by fibre fracture, matrix cracking and splitting.

5.2 Notched I-beams

A preliminary test was conducted on a web-notched carbon/epoxy I-beam which had both a circular and a diamond cutout machined into its two shear loaded regions, with the notches being centrally located along the neutral axis of the beam and between the outer pairs of loading pads. The circular notch was 46 mm in diameter, whilst the diamond notch had 46 mm diagonal lengths and a 4·36 mm corner radius. The maximum dimensions of these notches did not exceed 40% of the internal web depth, and the circular notch was some 26% larger in area than the diamond cutout. Failure of the beam occurred at the circular notch without any damage being caused at the diamond notch. Consequently, it was decided to test all subsequent notched beams using the more severe of these cutouts, i.e. only using circular notches. Both 46 and 60 mm diameter holes were drilled into the shear loaded regions of the web of the I-beams, see Fig. 3(b). It was around the larger diameter cutouts that damage and failure were concentrated in both the carbon/epoxy and glass/epoxy beams. The damage typically appeared as both tensile and compressive

damage due to the resolved stresses around the web notch. Damage was confined to the web region between the loading pads and was not evident in any other regions of the I-beams. It is not known whether the tensile damage preceded or was more catastrophic than the compressive damage in these notched static tests; however, in fatigue tests[27] on identical I-beams the tensile damage occurred before the compressive damage and extended radially outward from the cutout by a greater distance than the compressive damage.

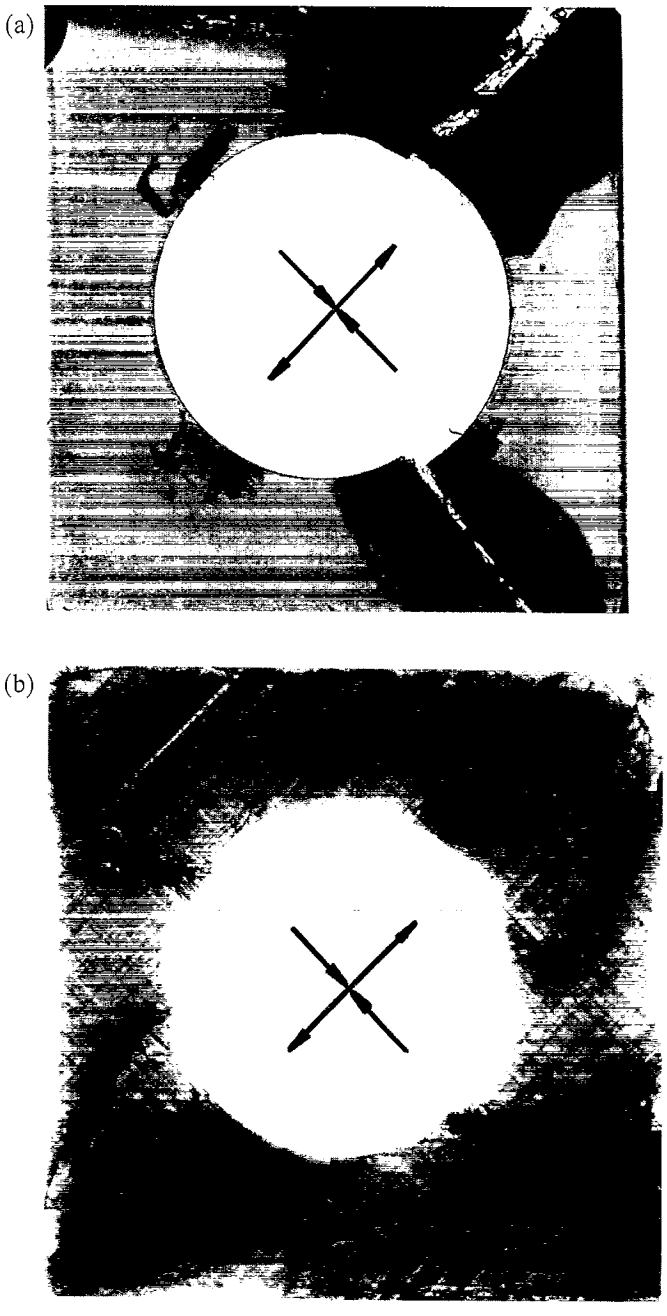

Fig. 16. The damage (delamination, matrix cracking, fibre fracture, splitting, etc.) that was detected around the large cutouts (60 mm diameter) in the web regions of (a) the notched carbon/epoxy I-beam and (b) the notched E-glass/epoxy I-beam using dye-penetrant enhanced X-radiography. In both cases, the compression flange is along the top of the photographs and the tension flange along the bottom. The local directions of resolved tensile and compressive stresses are indicated.

5.2.1 Carbon/epoxy compared with glass/epoxy I-beams

The damage that can be seen visually has already been detailed in Fig. 6, whilst Fig. 16 identifies the extent of damage and some of the different damage mechanisms that were detected using dye-penetrant enhanced X-radiography. The general appearance of the tensile and compressive damage in the carbon/epoxy and glass/epoxy beams is significantly different. The damage in the glass/epoxy beam is also more extensive than that associated with the carbon/epoxy beam. The tensile damage in the glass beam extends into two quadrants from the cutout, whilst the tensile damage in the carbon beam is confined to the quadrant adjacent to the tensile flange. Similarly, the compressive damage in the glass beam is present in two quadrants whereas the corresponding damage in the carbon beam is only in one quadrant adjacent to the compressive flange.

Dye-penetrants (dibromomethane and zinc iodide) were used in the X-ray studies of these components. It was not possible, therefore, to use scanning electron microscopy to examine the particular damage mechanisms in greater detail, in order to establish the reasons for the difference between the carbon and glass beam damage. Nor was it possible to use SEM to study the particular damage mechanisms that had occurred during the failure process.

However, it is thought that, since the failure strain of the E-glass fibres is some 2·4%,[40] compared with that of the carbon fibres being some 1·5%,[41] and since the matrix material in both components is the same Ciba Geigy 914 epoxy system, more matrix damage would indeed occur in the glass beam before final failure. Also, for both types of beam, the final failure is associated with fibre fracture. Consequently, it is reasonable to expect that more extensive damage would have been associated with failure of the notched E-glass/epoxy I-beam.

5.2.2 Damage mechanisms

The particular damage mechanisms that were identified, by visual examination, X-radiography and optical microscopy of various through-thickness sections around the web cutouts were matrix cracking, transverse ply cracking, fibre kinking and fibre fracture, delamination and splitting. Some of these mechanisms are shown in the optical micrographs of Figs 17 and 18. These figures are from microscopy sections that were taken at various distances from the edge of the holes, in order to develop a map of the damage mechanisms which were present through the thickness of the composite web, both near and away

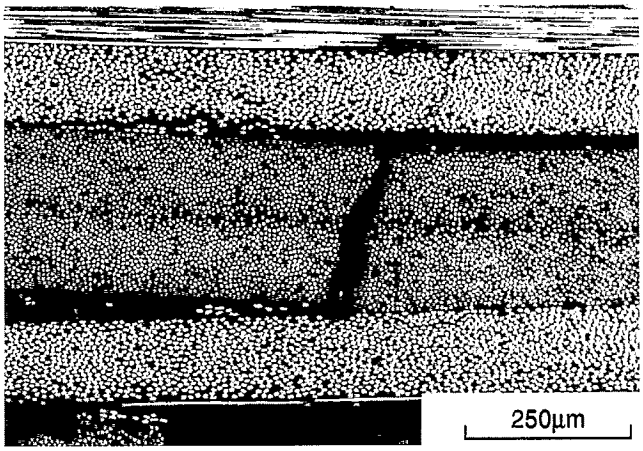

Fig. 17. Optical micrograph of the through-thickness damage typically identified ahead of the large web cutout (60 mm diameter). A single continuous matrix crack is present in two local 90°/90° plies (global −45°/−45° plies) subjected to local tensile stresses. This matrix crack joins delaminations that are present along two 45°/90° interfaces. Some matrix cracking is also evident in the 45° plies. Each ply has a nominal thickness of 0·125 mm.

from the holes. Whilst all the aforementioned damage mechanisms were present at the boundary of the holes, only matrix cracking and delamination were present at a distance of some few ply thicknesses away from the boundary of the holes. Moreover, the density of matrix cracking in any given ply decreased rapidly with distance away from the hole. It was found that matrix cracks dominated in local 90°/90° plies which were subjected to tensile stress, and a typical micrograph is shown in Fig. 17. Nairn [42–44] has also shown that, in similar laminates, matrix cracking will

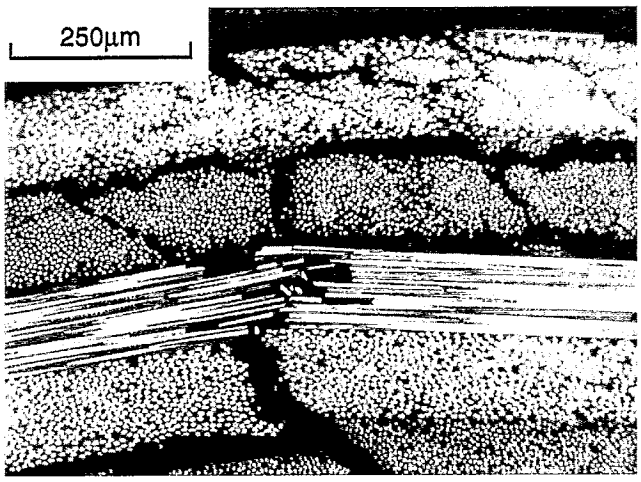

Fig. 18. Optical micrograph of the through thickness damage typically identified ahead of the large web cutout (60 mm diameter). Fibre fracture of a local 0° ply (global 45° ply) is evident, together with delamination along local 45°/90° and 0°/90° interfaces, and matrix cracking and intraply cracking of local 90° and 45° plies. These plies are subjected to local tensile stresses. Each ply has a nominal thickness of 0·125 mm.

predominate in these plies. (Note that these local 90°/90° plies were global −45°/−45° plies.) Figure 18 identifies the damage present in different plies at a location closer to the hole edge than Fig. 17. Fibre fracture within a 0° ply, delaminations along a 0°/90° and two 90°/45° ply interfaces, and both matrix cracking and intraply cracking of 90° and 45° plies are all evident.

5.2.3 Summary

In summary, all damage initiated from the free edge of the web cutout where the stress concentration factor was greatest. It is not known whether the compressive or the tensile damage mechanisms occurred first in these statically tested I-beams. Similarly, it is not known whether the damage mechanism which was responsible for ultimate failure was due to tensile or compressive stresses.

6 CONCLUSIONS

The most significant damage mechanisms which were present in the I-beams were delamination, matrix cracking, splitting and fibre fracture.

In the unnotched I-beams the major delaminations occurred along +45°/−45° interfaces (in particular between the backs of the two channel sections and between the flange caps and the channel sections) with secondary delaminations occurring between interfaces of 45° relative angular orientation, e.g. see Figs 2, 5 and 10. Damage initiated, in a predominantly mode I (i.e. tensile opening) manner (see Figs 5 and 7). The damage was observed as edge delaminations from the edges of the compression flanges which subsequently propagated in a mixed mode manner (i.e. under a mixture of tensile and shear stresses, see Figs 5 and 8) towards the fillet region. The edge delamination initiated at the crest of a local buckle on the compressive flange. Having reached the fillet region of the unnotched I-beams (see Figs 5, 10 and 11), the delamination propagated through the web (see Figs 5, and 12–14) and towards the tension flange of the I-beams, again in a mixed mode manner. The fractographic evidence indicated that the mixed mode fracture was at different ratios of mode I/II in the flange and web regions of the I-beams.

Failure of the notched beams was localised around the large (i.e. 60 mm diameter) shear-loaded web cutouts, see Figs 3(b), 6 and 16. Extensive delamination, caused by local compressive stresses, was present around the web notch (see Fig. 16). Matrix cracking, splitting and fibre fracture (see Figs 16–18) were also present and had been caused by local tensile stresses. Matrix cracking in local 90°/90° plies (see Fig. 17), which was caused by local tensile stresses, initiated at the edge of the web notches and subsequently propagated to the tensile and compres-

sive flanges (see Fig. 6). Through-thickness cracking, splitting and fibre breakage were all a consequence of this initial matrix cracking damage. However, it is not known whether the compressive or the tensile damage mechanisms occurred first within the I-beams. Similarly, it is not known which of the tensile or compressive damage mechanisms led to final catastrophic fracture of the I-beams.

This detailed knowledge of the damage mechanisms from the I-beams which failed under statically applied loads will be used to identify the damage mechanisms observed under cyclic fatigue loading of the I-beams. Further, this information will be employed in a future paper[39] to construct a micromechanical model for predicting the fatigue lifetime of structural components.

ACKNOWLEDGEMENTS

The authors acknowledge the financial assistance of British Aerospace plc, the DTI (via the LINK 'Structural Composites' programme), EI Du Pont de Nemours and Co. Inc., Rolls Royce plc, SERC (now EPSRC), Shell Research and Westland Helicopters Ltd as well as the advice of Prof. P. Curtis of DRA, Farnborough. This work was performed when M.D.G. was at Imperial College. The advice and assistance of Mr E. Greenhalgh of the DRA, Farnborough, and Mr N. Svensson of the Swedish Institute for Fibre and Polymer Research with aspects of fractography and of Mr E. W. Godwin and Mr H. J. MacGillivray, of Imperial College, with experimental aspects of this programme is acknowledged.

REFERENCES

1. Purslow, D., Some fundamental aspects of composites fractography. Royal Aircraft Establishment, Technical Report 81127, 1981.
2. Purslow, D., Fractographic analysis of failures in CFRP. *Characterisation, Analysis and Significance of Defects in Composite Materials*, AGARD, Conf. 355M, London, 1983, pp. 1.1–1.11.
3. Purslow, D. Composites fractography without an SEM—The failure analysis of a CFRP I-beam. *Composites*, **15** (1984) 43–48.
4. Purslow, D., Matrix fractography of fibre–epoxy composites. Royal Aircraft Establishment, Technical Report 86046, 1986.
5. 'tHart, W. G. L., Scanning electron microscopy of fracture surfaces of carbon composite materials. *NLR TR* 76035 *U*, National Aerospace Laboratory, The Netherlands, 1976.
6. Miller, A. G. & Wingert, A. L., Fracture surface characterization of commercial graphite/epoxy systems. *Nondestructive Evaluation and Flaw Criticality for Composite Materials,* ASTM STP 696, ed. R. B. Pipes. American Society for Testing and Materials, Philadelphia, PA, 1979, pp. 223–273.
7. Morris, G. E., Determining fracture directions and fracture origins on failed graphite/epoxy surfaces. *Nondestructive Evaluation and Flaw Criticality for Composite Materials,* ASTM STP 696, ed. R. B. Pipes. American Society for Testing and Materials, Philadelphia, PA, 1979, pp. 274–297.
8. Hibbs M. F. & Bradley, W. L., Correlations between micromechanical failure processes and the delamination toughness of graphite/epoxy systems. *Fractography of Modern Engineering Materials*: *Composites and Metals,* ASTM STP 948, ed. J. E. Masters & J. J. Au. American Society for Testing and Materials, Philadelphia, PA, 1987, pp. 68–97.
9. Bradley, W. L., Relationship of matrix toughness to interlaminar fracture toughness. *Application of Fracture Mechanics to Composite Materials*, ed. K. Friedrich. Elsevier, Amsterdam, 1989, pp. 159–187.
10. Richards-Frandsen, R. & Naerheim, Y., Fracture morphology of graphite/epoxy composites. *J. Comp. Mater.*, **17** (1983) 105–113.
11. Donaldson, S. L., Fracture toughness testing of graphite/epoxy and graphite/PEEK composites. *Composites*, **16** (1985) 103–112.
12. Johannesson, T., Sjöblom, P. & Seldén, R., The detailed structure of delamination fracture surfaces in graphite/epoxy laminates. *J. Mater. Sci.*, **19** (1984) 1171–1177.
13. Morris, G. E., Determining fracture directions and fracture origins on failed graphite/epoxy surfaces. *Nondestructive Evaluation and Flaw Criticality for Composite Materials*, ASTM STP 696, ed. R. B. Pipes. American Society for Testing and Materials, Philadelphia, PA, 1979, pp. 274–297.
14. Johannesson, T. & Blikstad, M., Fractography and fracture criteria of the delamination process. *Delamination and Debonding of Materials*, ASTM STP 876, ed. W. S. Johnson. American Society for Testing and Materials, Philadelphia, PA, 1985, pp. 411–423.
15. Arcan, L., Arcan, M. & Daniel, I. M., SEM fractography of pure and mixed-mode interlaminar fractures in graphite/epoxy composites. *Fractography of Modern Engineering Materials*: *Composites and Metals,* ASTM STP 948, ed. J. E. Masters & J. J. Au. American Society for Testing and Materials, Philadelphia, PA, 1987, pp. 41–67.
16. Lee, S. M., Fractography of composite materials. *International Encyclopedia of Composites, Vol* 2. VCH Publishers, 1990, pp. 268–289.
17. Smith, B. W. & Grove, R. A., Determination of crack propagation directions in graphite/epoxy structures. *Fractography of Modern Engineering Materials*: *Composites and Metals,* ASTM STP 948, ed. J. E. Masters & J. J. Au. American Society for Testing and Materials, Philadelphia, PA, 1987, pp. 154–173.
18. Friedrich, K., Fractographic analysis of polymer composites. *Application of Fracture Mechanics to Composite Materials*, ed. K. Friedrich. Elsevier, Amsterdam, 1989, pp. 425–487.
19. Russell, A. J. & Street, K. N., The effect of matrix toughness on delamination: Static and fatigue fracture under mode II shear loading of graphite fibre composites. *Toughened Composites*, ASTM STP 937, ed. N. J. Johnston. American Society for Testing and Materials, Philadelphia, PA, 1987, pp. 275–294.
20. Carlsson, L. A., Trethewey, B. R. & Gillespie, J. W., Mode II cyclic delamination growth. *J. Comp. Mater.*, **22** (1988) 459–483.
21. Gilchrist, M. D. & Svensson, N., A fractographic analysis of delamination within multidirectional carbon/epoxy laminates. *Comp. Sci. Technol.*, **55** (1995) 195–207.

22. Greenhalgh, E. S., Characterisation of mixed mode fracture in unidirectional laminates. Defence Research Agency, Contractor Report FMC CR941003, 1994.
23. Lowe, A. E., Structure and matrix dominated properties of T300/914 carbon epoxy composites. PhD thesis, Department of Material Science and Metallurgy, Cambridge University, 1992.
24. Greenhalgh, E. S., Mechanical evaluation of carbon-fibre reinforced thermoplastic I-beams. Defence Research Agency, Technical Report 92071, 1993.
25. Gamziukas, V., Skjuvprov med I-balkar av kolfiberarmerad plast med urtag i livet. FFA Report TN 1986-78, Aeronautical Research Institute of Sweden (FFA), 1986 (in Swedish).
26. Hollmann, K., Failure analysis of a shear loaded graphite/epoxy beam containing an irregular cutout. *Engng. Fract. Mech.*, **39** (1991) 159–175.
27. Gilchrist, M. D., Kinloch, A. J. & Matthews, F. L., Mechanical performance of carbon-fibre and glass-fibre-reinforced epoxy I-beams: III—Fatigue behaviour (in prep.).
28. Gilchrist, M. D., Kinloch, A. J., Matthews, F. L. & Osiyemi, S. O., Mechanical performance of carbon-fibre and glass-fibre-reinforced epoxy I-beams: I. Mechanical behaviour. *Comp. Sci. Technol.* (in press).
29. *LAP*: *Laminate Analysis Program*, Centre for Composite Materials, Imperial College, London, 1991.
30. Curtis, P. T. (ed.), CRAG test methods for the measurement of the engineering properties of fibre reinforced plastics. Royal Aircraft Establishment Technical Report 88012, 1988.
31. Kaczmarek, H., Ultrasonic detection of the development of transverse cracking under monotonic tensile loading. *Comp. Sci. Technol.*, **46** (1993) 67–75.
32. Davies, P., The effect of temperature on the interlaminar fracture of tough composites. *Proc. 6th Int. Conf. on Composite Materials (ICCM-VI)*, Vol. 3. Elsevier, London, 1987, pp. 3284–3294.
33. Hamada, H., Ramakrishna, S. & Sato, H., Effect of testing temperature on the energy absorption behavior of carbon fibre/PEEK composite tubes. *J. Reinf. Plast. Comp.*, **15** (1996) 30–47.
34. Hull, D., A unified approach to progressive crushing in fibre reinforced composite tubes. *Comp. Sci. Technol.*, **40** (1991) 377–421.
35. Farley, G. L. & Jones, J. M., Analogy for the effect of material and geometrical variables on energy-absorption capability of composite tubes. *J. Comp. Mater.*, **26** (1992) 78–89.
36. Hamada, H., Coppola, J. C., Hull, D., Maekawa, Z. & Sato, H., Comparison of energy absorption of carbon/epoxy and carbon fibre/PEEK composite tubes. *Composites*, **23** (1992) 245–252.
37. Shikhmanter, L., Cina, B. & Eldror, I., Fractography of multidirectional CFRP composites tested statically. *Composites*, **22** (1991) 437–444.
38. Bascom, W. D., Boll, D. J., Fuller, B. & Phillips, P. J., Fractography of interlaminar fracture of carbon-fibre epoxy composites. *J. Mater. Sci.*, **20** (1985) 3184–3190.
39. Gilchrist, M. D., Kinloch, A. J., Matthews, F. L. & Wang, Y., Mechanical performance of carbon-fibre and glass-fibre-reinforced epoxy I-beams: IV—Finite element predictions (in prep.).
40. Agarwal, B. D. & Broutman, L. J., *Analysis and Performance of Fibre Composites*, Wiley, 1990.
41. Lovell, D. R., *Carbon and High Performance Fibres Directory*, 5th edn. Chapman and Hall, 1991.
42. Nairn, J. A., Hu, S. & Bark, J. S., A critical evaluation of theories for predicting microcracking in composite laminates. *J. Mater. Sci.*, **28** (1993) 5099–5111.
43. Nairn, J. A. & Hu, S., Matrix microcracking. *Damage Mechanics of Composite Materials*, ed. R. Talreja. Elsevier, 1994, pp. 187–243.
44. Nairn, J. A., Some new variational mechanics results on composite microcracking. Proc. ICCM 10, Whistler, BC, Canada, 14–18 April 1995.